



## Linear and Nonlinear Shock Attenuation of Aqueous Methylcellulose Solutions



Yonatan Rotbaum<sup>a,8,\*</sup>, Galit Parvari<sup>b,8</sup>, Yoav Eichen<sup>b</sup>, Daniel Rittel<sup>a</sup>

<sup>a</sup> Faculty of Mechanical Engineering, Technion, Haifa, 3200008, Israel

<sup>b</sup> Schulich Faculty of Chemistry, Technion, Haifa, 3200008, Israel

### ARTICLE INFO

#### Keywords:

Aqueous methylcellulose  
Thermoreversible gelation  
Energy absorption  
Attenuation coefficient  
Dynamic loading

### ABSTRACT

Aqueous methylcellulose solutions are fascinating inverse-freezing materials, known to reversibly form gels upon heating. Recently, these materials have been found to undergo this endothermic solidification upon impact. The impact-induced solidification was shown to occur in the microseconds' timescale, setting the path for examining their functionality for shock absorption purposes. This present work focuses on characterizing the ability of methylcellulose solutions to mitigate impact forces, and on quantifying their attenuation coefficients for weak ultrasonic pulses as well as violent impacts. Ultrasonic attenuation measurements at temperatures higher than the gelation temperature (solid gel), reveal unique behavior which is attributed to the thermogelation mechanism. Impact experiments on 2 cm thick solutions have shown unexpectedly strong force and impulse mitigation, along with a high attenuation coefficient that grows exponentially with frequency. This attenuation performance was even further improved by increasing the concentration of gel-forming material. Reducing the thickness of the sample to 1 cm does not apparently reduce the force and impulse mitigation characteristics from those measured for 2 cm thickness, which is a distinct "anomaly" of materials used for wave mitigation. These observations imply that in the materials investigated herein, the main mechanism of shockwave attenuation is the sol→gel phase-transition, in contrast to shockwave passage through the viscous material bulk. Thus, the common normalization of the attenuation coefficient to the thickness of the medium is not valid for these materials.

### 1. Introduction

Upon impact, detonation, strong vibrations or hard collision between bodies, a significant amount of energy is transferred to the impacted structure by means of elastic stress waves. Blunt shock trauma caused by stress waves significantly raised the percentage of casualties of U.S army veterans who were exposed to explosion blast waves in short and intermediate range in Afghanistan and Iraq. [1,2]. Since the impact to the body was caused by airborne shock waves, there was no visual evidence for injury or hematoma, but the damage to the internal organs was severe in many cases. [3–6]. A similar effect was observed in American football and combat sports, where many young active players suffered from irreversible brain damage following blunt shock [7,8]. Similarly, marathon athletes are known to suffer from spine injuries due to the repeated shocks that each and every step imparts to the body [9]. The potentially devastating effect of stress waves has led to an extensive investigation of the phenomenon and development of

engineering techniques to mitigate the energy, or to isolate the object intended to be protected from these shockwaves.

Nowadays there are many different methodologies and techniques to attenuate impact and mitigate energy transfer, both at the design and the material selection levels. In terms of design, one can find plastically collapsing mechanisms [10–14]. Multiple layer composites can take advantage of the layers' different acoustic impedances, such as to reflect most of the incoming energy [15–19]. Moreover, the thickness of each layer can be tuned to reduce the bandwidth of the transmitted signal [15,20]. Alternatively, one can find porous media in which the porosity acts to reflect and dissipate incoming stress waves [11,21,22].

At the material level and in the mechanical design concepts, most suspension and shock absorbing devices are based on springs and dampers. Here, the spring is the load bearing component and the damper absorbs energy with a proportional relation to the impact velocity. Viscoelastic materials like polymers, rubbers and gels, act similarly, the spring is the material storage modulus, and the energy

\* Corresponding author.

E-mail address: [y.rotbaum@gmail.com](mailto:y.rotbaum@gmail.com) (Y. Rotbaum).

<sup>§</sup> Equal contribution

absorption determined by the viscosity and the loss modulus [23–25]. The versatility and the ability to control and modify many of the properties of these materials render them favorite candidates for many engineering applications [19,26–30]. Another concept in the materials group, are shock absorbing liquids. These liquids are usually highly viscous and nonNewtonian, hence rapid shocks lead to significant hardening, which does not necessarily imply shock mitigation [31–33]. Another type of material recently proposed for study in the context of shock attenuation is an inverse freezing liquid [34].

Inverse freezing materials are unique in their ability to undergo liquid to solid transition upon heating [35]. In a previous report, we have demonstrated how one such system – aqueous methylcellulose (AMC) gels not only harden when heated beyond their gelation point, but also respond to dynamic compression by a considerable increase in their flow stress [36]. More recently, we reported that room-temperature solutions of these materials undergo impact-induced gelation [34]. This very fast phase transition enables the uptake of the impact energy, and translates it into chemical energy, raising the possibility of using such materials as shockwave energy attenuators. However, the energy-mitigation properties of these aqueous solutions remained mostly uncharacterized.

Here we report on a study of the shock attenuation of AMC solutions in their liquid state, at room temperature. The investigation includes these materials' attenuation performance with respect to the loading regime, methylcellulose (MC) concentration and thickness of the absorbing layer. The properties of the material of interest, 5.6% wt. AMC, were compared to those of pure water, and 5% and 20% ballistic gelatin (BG). Our choice of these control materials was dictated by the fact that water composes 90–95% of AMCs and is known as a non-dissipative material with minimal attenuation of sound waves. 20% ballistic gelatin, on the other hand, is one of the most commonly tested materials in impact studies due the similarity of its mechanical properties to those of human tissues [37–41]. This report is the first to expand on the novel phenomenon of shock attenuation by AMCs, and explores the effect of basic factors which have not yet been examined, but which can nonetheless have considerable contribution to both the mechanistic understanding of how the attenuation occurs and also to the future implementation of these solutions into actual protective elements in engineering systems.

## 2. Experimental details

### 2.1. Materials and gel preparation

Methylcellulose (SG-A7C Food Grade, Dow Chemical Company, USA) and Ballistic Gelatin (Bloom 300, MM Ingredients, UK) were used as purchased, without further purification. Aqueous solutions of MC were prepared by heating ultrapure water (18 MΩ, 0.1 μm, Millipore Milli-Q instruments) to 70 °C and then adding the required amount of methylcellulose powder for a given concentration. The mixture was then stirred vigorously, at 70 °C, for at least five more minutes. The mixture was then transferred to an ice-bath for one hour, followed by incubation for at least 12 h at 4–8 °C, before use. 5% wt. and 20% wt. ballistic gelatin was prepared similarly to the AMC, omitting the ice-bath stage.

### 2.2. Ultrasonic attenuation (Linear attenuation)

The ultrasound experimental setup used for measuring the linear attenuation coefficients consists of a high voltage ultrasonic pulser (Olympus 5058PR) and an ultrasonic longitudinal probe with a nominal frequency of 1 MHz (SIUI-1M-24). The measured ultrasonic signals were recorded using an oscilloscope (Agilent DSO-X 2004A, 2 Gsa/sec).

For the ultrasound measurements, AMC solutions were cast into a cylindrical PMMA holder,  $D_{\text{outer}} = 40$  mm (wall thickness of 3 mm), covered with a thin (0.2 mm) plastic slide as the lower plate, which was

practically transparent to the ultrasonic pulse. The lower plate was placed directly on the ultrasonic probe, and the measurements were performed using the pulse-echo technique [42–44]. The experimental setup is identical to the one used in previous work on A7C MC [36].

The recorded pulse-echo signal, was converted into rectified mode using Hilbert transform [45], and then each consecutive pulse was signed into an individual vector. The length of each vector of the pulse repetition was then artificially extended to a length of 2048 points using zero padding [46]. An example for raw ultrasonic signal and a calculated power spectrum are shown in Supplementary Material (Fig. 1S). For the frequency dependent attenuation coefficient, the pulses were compared in the frequency domain using fast Fourier transform. The expression of the attenuation coefficient ( $\alpha_1$ ) is given by Eq. (1) where  $X$  is the height of the material in the sample, and  $I_1$  and  $I_2$  are the intensity levels of two consecutive repetitions at a given frequency. Eq. (1):

$$\alpha_1(Np/cm) = \ln\left(\frac{I_1(f)}{I_2(f)}\right)/2X \quad (1)$$

The plots of attenuation coefficients as a function of the frequency presented in the paper are the results averaging at least 200 experiments. More detailed information on the attenuation calculation and the statistical error appears in the supplementary material. (Fig. 2S).

### 2.3. Nonlinear attenuation

The nonlinear attenuation experimental setup consists of two main parts: 1. a 12.7 mm diameter Hopkinson bar [47], made of 7075-T6 aluminum-alloy, and a 15 cm projectile made of the same material. 2. a liquid-containing chamber with internal dimensions of  $h = 93$  mm,  $w = 96$  mm,  $d = 20$  mm, made of 10 mm thick aluminum plates. (Fig. 1a and b) The rear plate of the box was connected to a tunable screw mechanism, so that thickness of the medium within the box could be varied. Experiments were conducted at thicknesses of 20 mm and 10 mm.

The impacting stress waves are generated by propelling the aluminum striker towards the Hopkinson bar, using a gas gun. As the striker hits the bar, an elastic stress wave starts to propagate towards the far edge of the bar, which is in contact with the gel-containing aluminum chamber. As the stress wave reaches the bar's far end/chamber interface, part of the wave continues to propagate in the original direction through the impacted wall of the chamber and into the AMC solution (transmitted wave) while the other part of the wave is reflected back into the bar (reflected wave). From the original incident and reflected stress pulses, the applied force on the aluminum chamber was calculated. (Eq. (2)) Where  $E_b$  is the bar's Young's modulus,  $A_b$  is the bar's surface area and  $\varepsilon_i$  and  $\varepsilon_r$  are the incident and the reflected stress waves respectively. Eq. (2):

$$F_{in} = A_b E_b (\varepsilon_i + \varepsilon_r) \quad (2)$$

During the experiments the recorded impacted forces were in the range of 2500–22,000 N. An example of typical force profiles recorded on the Hopkinson bar is shown in Fig. 3S (see supplementary material).

The transmitted wave propagating through the medium filling the chamber was recorded by a set of two A201 FlexiForce™ sensors, as described previously [36,48,49]. One sensor was placed on the inner side of the impacted (front) wall of the chamber and the other was placed on the rear (far) wall of the chamber. This allowed for load recording on both sides of the investigated gel. The impact attenuation calculation was performed according to the same procedure as the ultrasonic attenuation. The force profiles (before and after the liquid filler) recorded using the Flexi-force sensors can be compared to two consecutive ultrasonic pulses (Figure S1). These force profiles were converted to power spectra using a Fourier transform (intensity vs frequency). Finally the attenuation coefficient is calculated according to

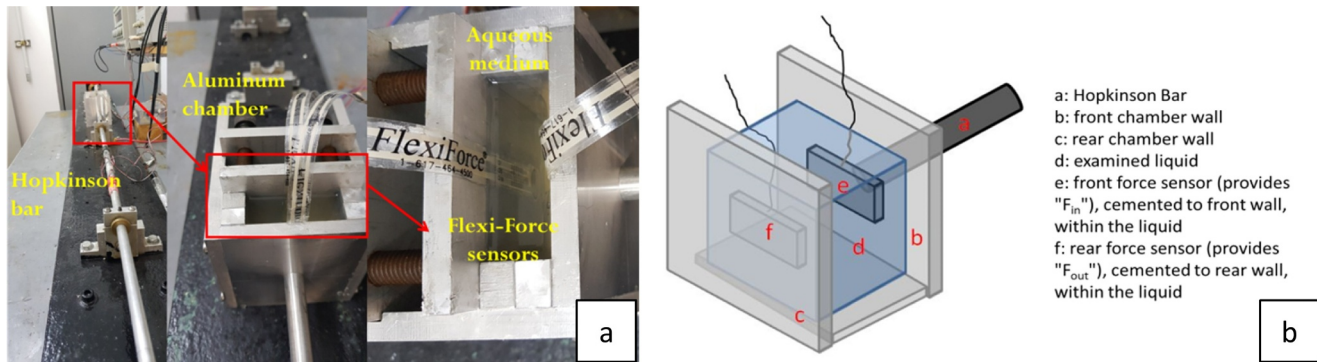


**Fig. 1.** Experimental setup for nonlinear attenuation measurements. (a) From left to right: Hopkinson bar and a top/front view of the impacted chamber. The front plate of the impacted chamber is in contact with the Hopkinson bar; top view of the contents of the chamber, with the placement of the Flexi-Force™ sensors.(b) a scheme of the experimental system.

#### Eq. (1).

Prior to each experiment, the chamber and the solution were thermally equilibrated at  $23 \pm 2$  °C. More than 50 repetitions were conducted for each material concentration and thickness.

### 3. Results

The results are divided into linear and nonlinear attenuation. The terminology of the sections originates from two main reasons. Soft materials at low frequencies ( $\sim <5$  MHz) are known to exhibit a positive linear correlation between the attenuation coefficient and the frequency [50–54]. In addition, linear elasticity theory applies to small amplitude deformations, such as those excited by ultrasound [55,56]. In contrast, Hopkinson bars generate large amplitude stress/shock waves [47,57,58], which are likely to cause a nonlinear material response. Any attenuation caused by nonlinear strains will hereby be referred to as nonlinear attenuation.

#### 3.1. Linear attenuation

The attenuation calculation was performed by dividing the intensity at any given frequency of two consecutive pulse repetitions. The resulting averaged attenuation coefficient was found to be of a similar value when compared between different pairs of pulse repetitions. The calculated average attenuation coefficient of the different tested solutions is shown in Fig. 2.

As a general remark, except for water which is not considered as a viscous fluid, the attenuation increases with frequency. As shown in

**Table 1**

Averaged attenuation coefficients at frequencies of 500KHz and 950KHz, as measured for water, 5% BG, 20% BG, 10% AMC, 5.6% AMC at room temperature and 5.6% AMC gel at 80 °C.

Material	Water	5% BG	20% BG	5.6% AMC	5.6% AMC gel	10% AMC
$\alpha_1$ (Np/cm) (500KHz)	0.005	0.0097	0.23	0.15	0.53	0.54
$\alpha_1$ (Np/cm) (950KHz)	0.003	0.10	0.78	0.22	0.72	0.91

**Fig. 2.**, the attenuation coefficient of water is approximately 0.005 Np/cm with almost no frequency dependence. The measured attenuation coefficients of the tested materials are summarized in Table 1. Note that the measured value for BG was found to be in good agreement with literature.

The viscosity of BG and AMC increases with increase in concentration of these solutions, as found in previous rheological measurements [59–61]. This correlates well to the expectations from a more viscous medium, which should exhibit higher attenuation as shown in the 5% wt. AMC heated gel compared to the 5% AMC solution.

In contrast to the expectation due to viscosity considerations, the chemical considerations lead to the opposite expectation. Based on the energy-consuming sol $\rightarrow$  gel transformation, it is expected that the liquid would show higher attenuation performance than the gel, due to the gel having less polymers available to undergo gelation. A possible

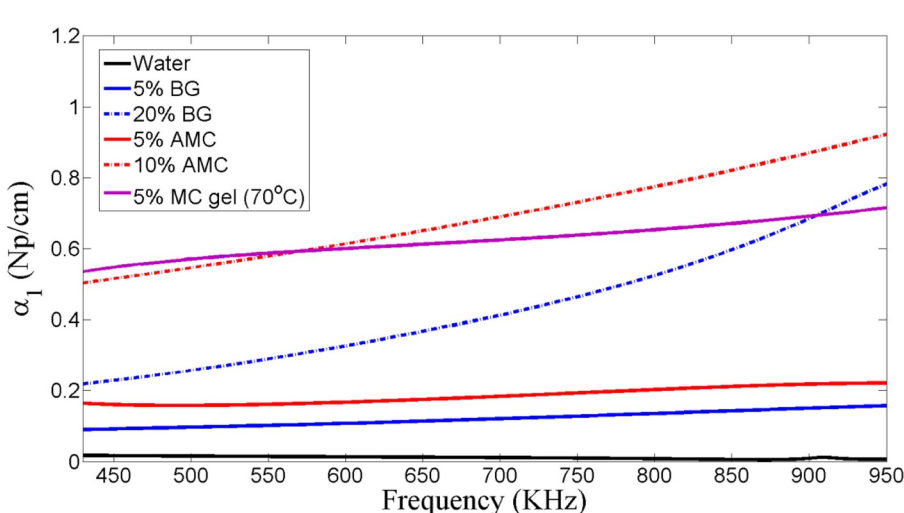


**Fig. 2.** Averaged attenuation coefficients as a function of the frequency, of the different tested materials.

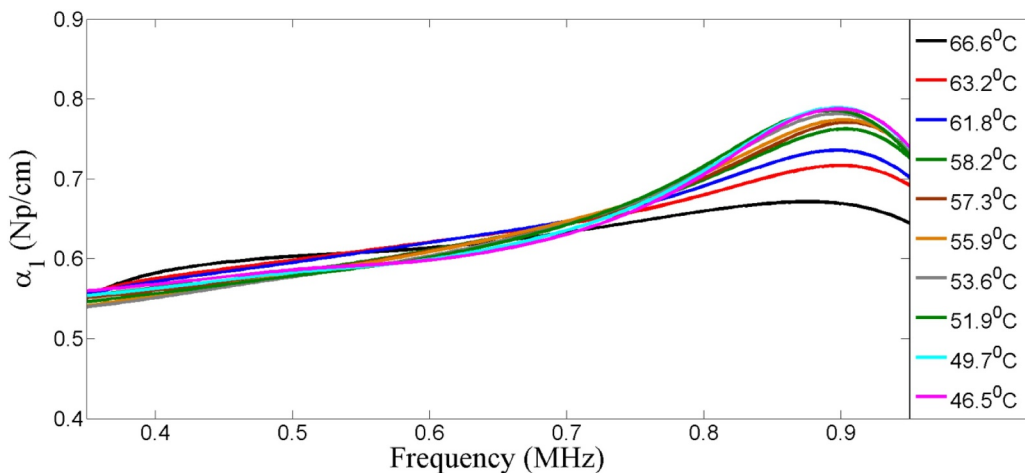


Fig. 3. Averaged attenuation coefficients as a function of the frequency, of 5.6% AMC as it cools down to room's temperature.

explanation to this supposed contrast would most likely rely on the structure of the gel, which has been shown to include fibrils of varying length and near constant diameters of about 15 nm [60,62]. Unfortunately, it is yet to be discovered how such fibrils further associate with each other and possibly other structural elements, to form the macro-sized organic structures which exist in the gel. These latter are at least large enough to scatter light in the visible wavelengths, to form opaque gels in their heated form. Thus, how the ultrasound waves, having wavelengths of 3.5 mm and 1.6 mm at frequencies of 450 and 950 Hz respectively, interact with the structures of the gel is currently unknown.

These results motivated the exploration of the dependence of the attenuation coefficient, on the temperature of the AMC solution. For this purpose, two identical sealed 5.6% MC samples were kept at  $\sim 85^{\circ}\text{C}$  for 20 min. Then, one of the samples was used for attenuation measurements while the other was used for temperature measurements using a thermocouple inserted into the bulk of the gel. Immediately after the heating stage, one sample was placed on the ultrasonic probe and the second was placed on a similar probe in close proximity to the first sample, in order to replicate the heat loss from the first sample. The frequency dependent attenuation coefficients of the 5.6% MC sample at different temperatures, as it cooled down, are shown in Fig. 3.

As shown in Fig. 3, as the gel cools down from  $66.6^{\circ}\text{C}$  to  $58.2^{\circ}\text{C}$ , there is a significant increase of the measured attenuation, at frequencies in the range of 0.75–0.95 MHz. The studied temperature range is above the gelation point ( $T_g$ ) of the sample,  $42^{\circ}\text{C}$  [36]. Several earlier studies have shown considerable hysteresis of the  $T_g$  between heating processes (sol→gel) to cooling processes (gel→sol) of these materials [63,64], which lowers the  $T_g$  in the cooling process by more than  $10^{\circ}\text{C}$  compared to the  $T_g$  found on heating. It was also found that on cooling  $T_g$  shows relatively little dependence on the rate of cooling and on the MC concentration in the solution. Thus, over the temperature range reported, the  $T_g$  was not reached in our sample, and the changes in attenuation observed for the sample at  $66.6^{\circ}\text{C}$  to  $58.2^{\circ}\text{C}$  are not due to the entire medium undergoing phase transition. We are currently exploring possible mechanisms to account for this observed behavior, in which the "cold" gel shows higher attenuation than the "hot" gel. We suggest that the mechanism relies on the interactions of solvated polymers with the existing gel network. When energy is provided to the gel, in this case in the form of ultrasound waves, these solvated polymers are "recruited" to the gel network in a local gelation process that uptakes the provided energy. Support for this possibility can be found in two previous findings: first, the gel heated beyond its  $T_g$  continues to harden [36]; second, the addition of rigid particles, which interact with the MC polymers and likely facilitate the recruitment of solvated polymers into the gel network in AMC hydrogels, increase this

temperature-hardening dependence [65]. This "recruitment" in the ultrasound-irradiated gels would be more considerable with the rise in solvated polymer population, which in turn is expected to grow in the lower temperature range of the existence of the gel structure. If indeed this occurs, it would fit the increase in attenuation with the lowering in temperature in this range. However, this mechanism still requires further evidential support, and why the phenomenon is observed at the frequency range between 0.75 MHz and 0.95 MHz still needs to be clarified.

### 3.2. Nonlinear attenuation

Nonlinear attenuation experiments are a direct follow-up to the newly found phenomenon of impact-induced gelation of AMC solutions [34]. In this previous report, we have demonstrated large mitigation of forces passing through this material, in correlation with the impact-induced endothermic phase transition. In this report, the impact forces studied are considerably larger, and the attenuation was measured by following three main parameters: the reduction of the maximum force amplitude measured by force sensors before and after the medium, the reduction of the transmitted impulse, and the attenuation coefficient itself as a function of the frequency. All these parameters are common measures in the standardization of protective gear [66–68].

The first set of experiments was conducted at a constant thickness, where the distance between the aluminum chamber walls was set to 2 cm. (Fig. 1a and b). In this set, all the loading force amplitudes remained within the range of 9–10 KN. Representative force amplitudes recorded on the force sensors for water, 5% ballistic gelatin and 5.6% AMC are shown in Figs. 4a-c. in which the signals have been shifted in time for them to coincide.

In the reference experiment, Fig. 4a, the forces recorded before and after the water are almost of the same amplitude. Since water is considered as non-attenuating material, we assume that the minor reduction in the force amplitude is due to the dissipation of the wave front that transitions from 1D when leaving the Hopkinson Bar into a 3D front upon interaction with the chamber structure. The averaged force reduction and impulse of the tested materials are summarized in Table 2.

In the ultrasound experiments, 5% BG and 5.6% AMC exhibit comparable attenuation coefficients. However, in the nonlinear experimental conditions, which are more similar to blunt shock generated by impact, the reduction of the load peak by the AMC is more than three times higher than that of the BG. This remarkable difference is tentatively ascribed to the mechanism of endothermic phase transition in AMC, as previously reported for systems with lower impact energies [34].

The power spectra of the force profiles reveal valuable information

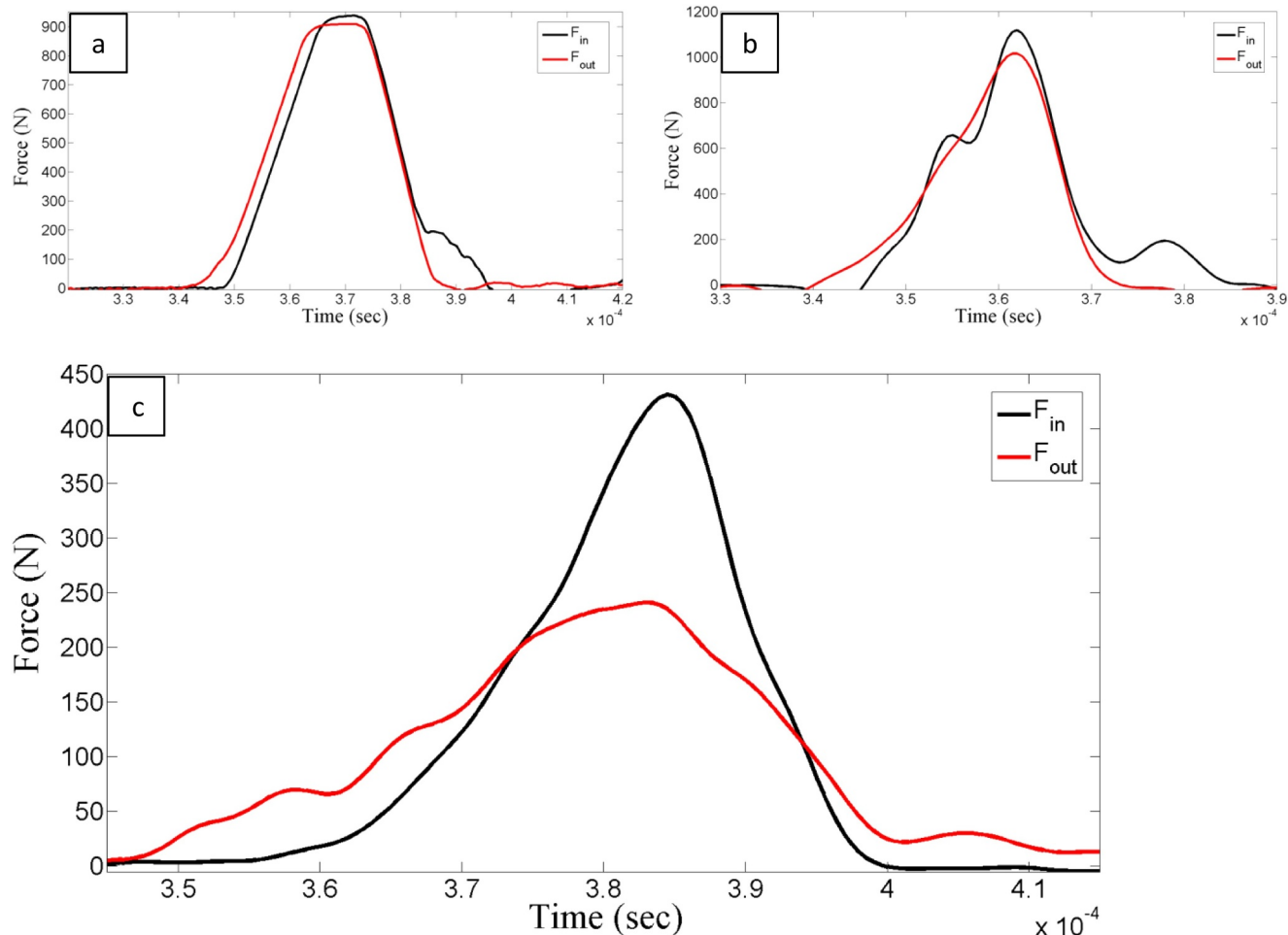


**Fig. 4.** Representative forces profiles recorded on the force sensors before and after the medium. (a) for water. (b) for 5% BG. (c) for 5.6%AMC. Note that the forces have been shifted according to the maximum amplitude and that the y axis amplitude is different for each figure.

**Table 2**

Averaged amplitude and impulse reduction together with the minimum and maximum calculated values for water, 5% BG and 5.6% AMC, based on 60 experiments per group.

Material	Amplitude force reduction (%)	Min/max Values (%)	Impulse reduction (%)	Min/max Values (%)
Water	3.1	[1.1 4.3]	3.2	[2.6 4.1]
5% BG	11.1	[7.8 16.7]	12.9	[9.1 18.5]
5.6% AMC	35.4	[29.1 40.3]	25.6	[22.1 33.5]

on the energy attenuation performance as a function of the frequency. (Figs. 5a–c).

Fig. 5a, shows again that water is an excellent reference material for calibration of the experimental setup with hardly any force mitigation. The power spectrum clearly shows that apart of a minor energy loss in frequencies of  $\sim 12$  KHz, the energy intensity is fully preserved. The power spectrum of BG (Fig. 5b) exhibits an almost constant ratio between the intensity levels before and after the BG over the tested frequencies range ( $\sim 43$  KHz). This observation implies that the attenuation coefficient is almost constant over these frequencies.

Fig. 5c shows that AMC is a considerably more potent energy mitigator than the other two examined materials. For frequencies in the range of 0–20 KHz the intensity ratio is about 60%. At frequencies higher than 20 KHz full attenuation is observed and there is practically no energy transmitted to the rear sensor.

Up to this point, all the presented impact experiments were

performed at relatively constant loading amplitudes of 9–10 KN. Additional experiments, which were conducted with higher loading amplitude ( $\sim 20$  KN) did not yield any new observations or different measured value values in water, BG, or 5.6% wt. AMC. For the sake of brevity, a comparison between different loading amplitudes will only be presented for 10% AMC.

### 3.3. On the influence MC concentration

Apart from the increased viscosity of AMC solutions, it was expected that increase in concentration of methylcellulose would lead to higher attenuation capabilities of the liquid. This is due to two main reasons: first, a linear relationship was previously found between the MC concentration and the enthalpy required for gelation [69]. Second, it has been well established that increase of polymer concentration lowers the  $T_g$ , thus lowering the threshold bar of the impact stimuli [63,70,71]. These properties led to the assumption that AMC solutions of larger concentrations were worth studying, as they are expected to be even better shock attenuators. A concentration of 10% wt. was chosen, as at higher concentrations, the material behaves like an inhomogeneous solid rather than a solution. While this behavior does not prevent it from serving as a successful shock mitigator, the aspiration in this work was to maintain a material that could be more easily compared to the 5% wt. AMC. In contrast to the 5% AMC, the 10% wt. solution displayed different attenuation performance for different impact loading amplitudes.

Representatives force amplitudes recorded before and after 2 cm of

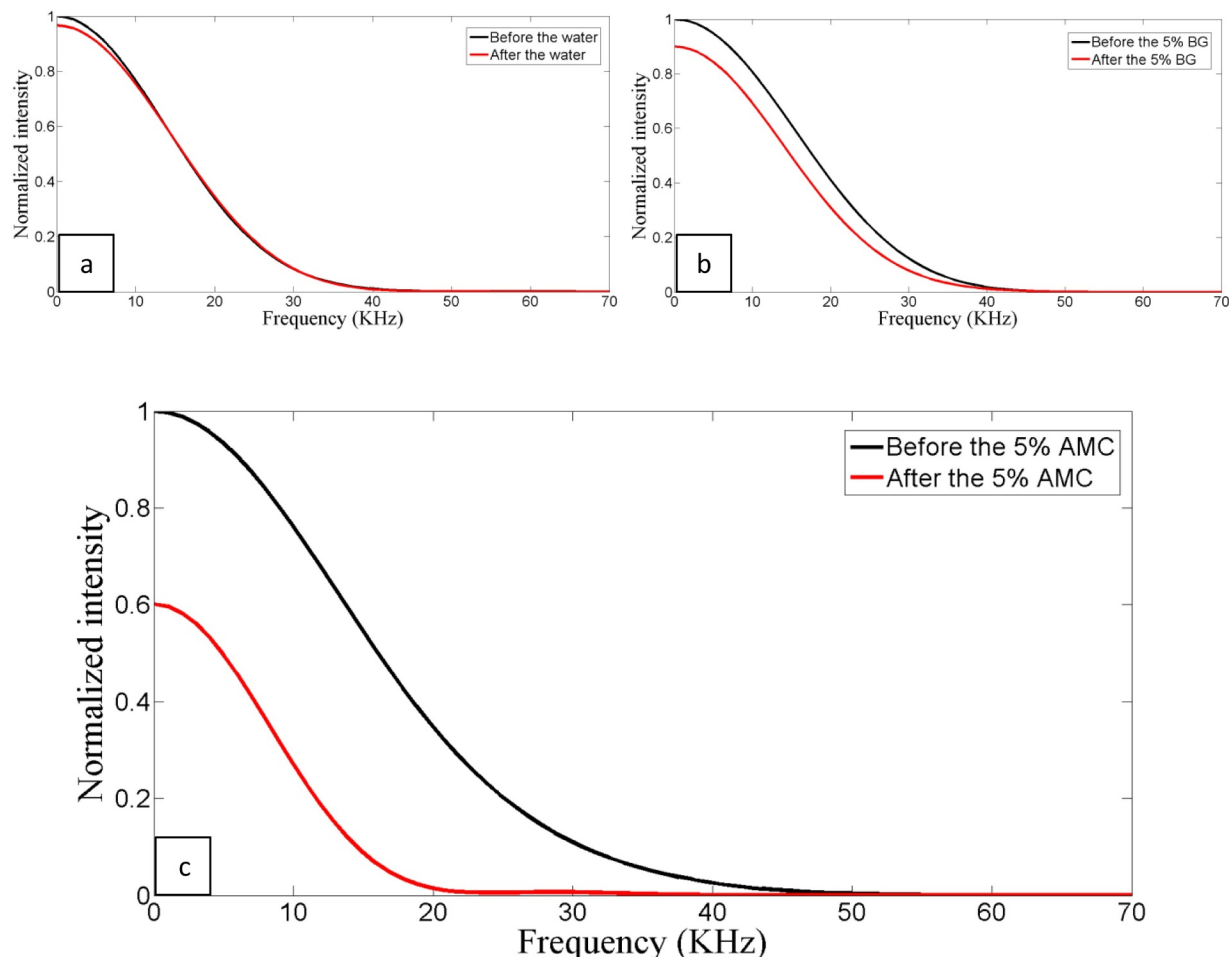


**Fig. 5.** Representative calculated power spectra from the force sensors before and after the medium. (a) for water. (b) for 5% BG. (c) for 5.6%AMC.

10% AMC submitted to impact loading amplitude of 10 and 20 KN are shown in Figs. 6a and b.

Figs. 6a and b shows two main changes in the "out force". Strong reduction in the force amplitude and the force profile is smeared over time in comparison to the profiles shown in Figs. 4a–c. For all of the tested loading amplitudes, the averaged force and impulse mitigation was found to be similar. The calculated averaged amplitude force reduction is now 65.5% [61.2–71.4%] and the impulse reduction is 43.5% [36.9–48.4%]. This significant improvement is the outcome of the addition of less than 5% MC to the previously studied AMC. However, this increment embodies more solvated polymers that would endothermically be able to gel upon impact. This increase in energy uptake capabilities, along with the reduction of  $T_g$ , correlates well to these

observations.

The calculated power spectra for the 10% AMC experiments submitted to loading impact amplitude of 10 and 20 KN are shown in Figs. 7a and b.

Figs. 7 shows that for impact loading amplitude of  $\sim 10$  KN, before the 10% AMC, the incoming signal spans up to a frequency of  $\sim 75$  KHz, while for 20 KN the frequency range reaches almost 200 KHz. Despite this difference in the incoming signals at the different loading amplitudes, the 10% AMC shows complete attenuation of both shockwaves at frequencies beyond  $\sim 60$  KHz. Another observation shown in Figs. 7 is that in both loading amplitudes, the ratio between the power spectrum curves before and after is very small, in the order of 20% or less.

A comparison between the response of the solution to both impacts

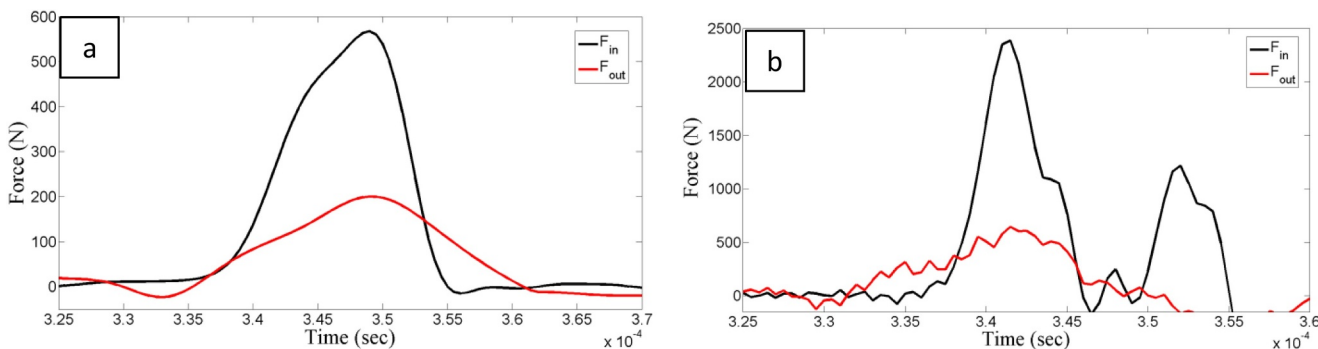


**Fig. 6.** Representative forces profiles recorded on force sensors before and after the 10% AMC. (a) loading amplitude of  $\sim 10$ KN. (b) loading amplitude of  $\sim 20$ KN. Note that the forces have been aligned according to the maximum amplitude and that the y axis is different between the different figures.

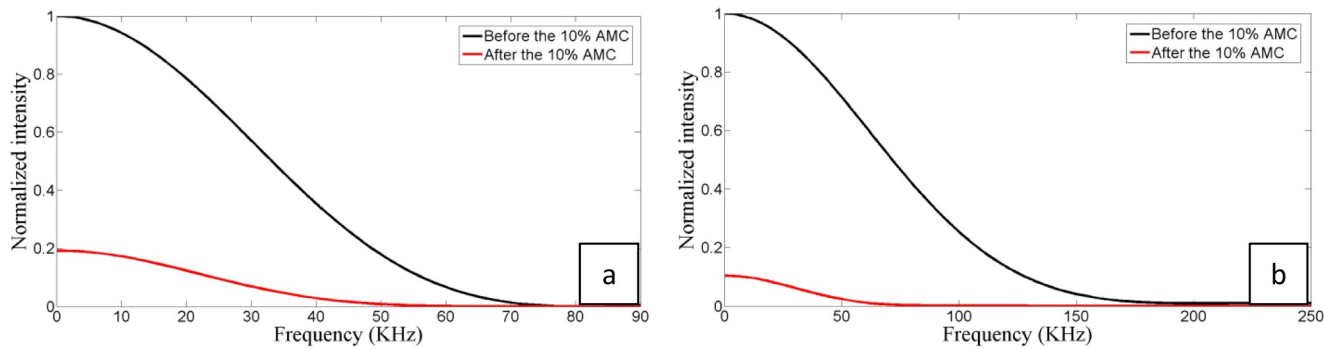


**Fig. 7.** Representative calculated power spectra from the force sensors before and after the 10% AMC. (a) loading amplitude of  $\sim 10\text{KN}$ . (b) loading amplitude of  $\sim 20\text{KN}$ .

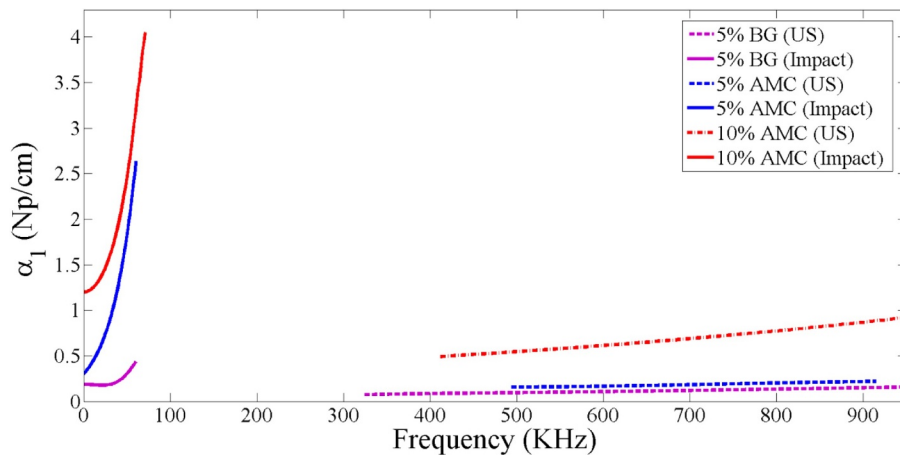


**Fig. 8.** Averaged nonlinear attenuation coefficients as a function of the frequency in comparison to the linear attenuation coefficient, of 5% BG, 5.6% AMC and 10% AMC.

amplitudes shows that the AMC's solutions exhibit an increased attenuation for the more powerful (energetic) impacts.

To summarize the results gathered so far from the impact experiments on different materials (at 2 cm thickness), the nonlinear and the linear attenuation coefficients are shown as a function of frequency in Fig. 8.

As shown in Fig. 8, the attenuation behavior is markedly different, for the different loading regimes. While ultrasonic attenuation displays a linear correlation with frequency, the impact attenuation exhibits a steep exponential dependence on the frequency.

### 3.4. On the influence of the AMC thickness

The forces profiles and the power spectrum of 1 cm thick water are shown in Figs. 9a and b.

According to the reference experiments shown in Fig. 9a, the force reduction decreased to  $1.5 \pm 0.5\%$  and the impulse reduction to  $1.0 \pm 1\%$  in comparison to  $3.6\%$  and  $3.1\%$  respectively at 2 cm. This behavior is expected from the reduction in the geometrical path between the two sensors, which leads to decreased dissipation of the stress wave. In the frequency domain, Fig. 9b shows that both lines have almost the same intensity amplitudes at all frequencies. The waviness of the amplitude originates from the strong impact of the Hopkinson bar on the box in addition to almost identical  $F_{\text{in}}$  and  $F_{\text{out}}$  amplitudes.

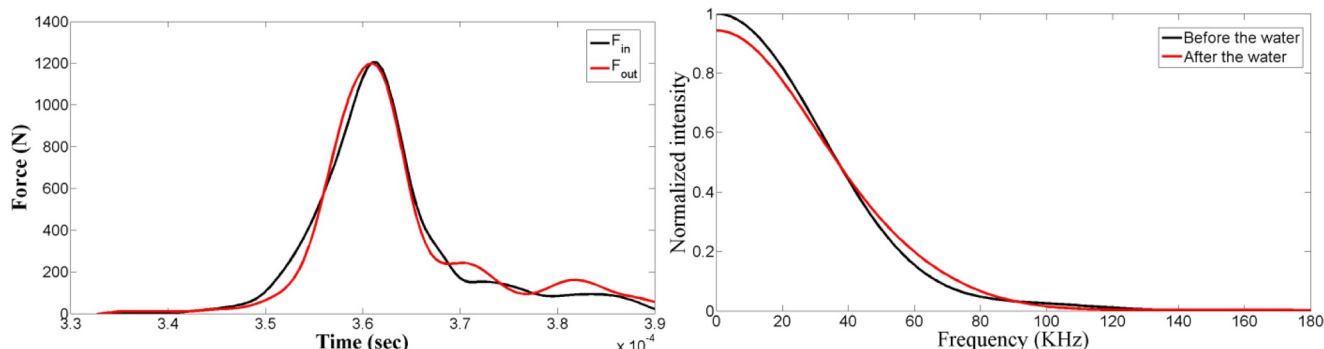


**Fig. 9.** (a) Representative forces profiles recorded using the force sensors before and after 1 cm thick layer of water. (b) Representative calculated power spectra from the force sensors before and after 1 cm thick layer of water.

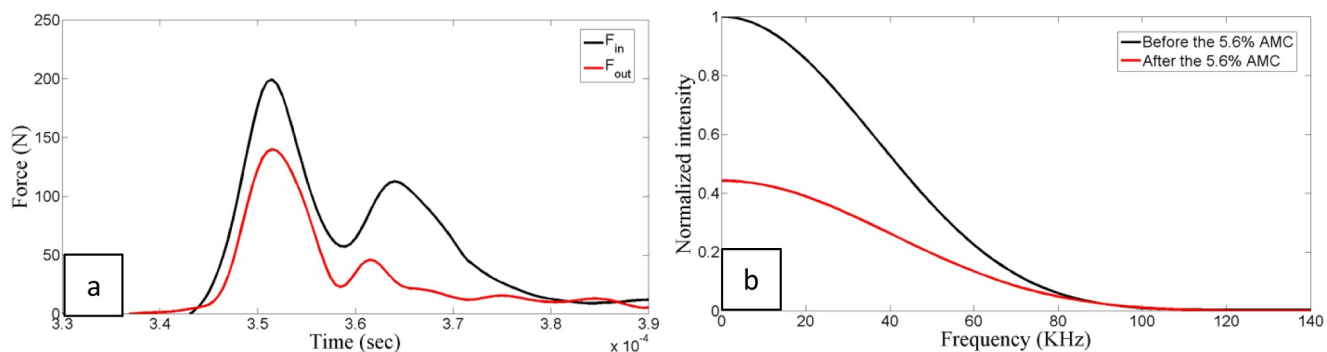


**Fig. 10.** (a) Representative forces profiles recorded on the force sensors before and after 5.6% AMC at thickness of 1 cm. (b) Representative calculated power spectra from the force sensors before and after 5.6% AMC at thickness of 1 cm.

1 cm thick 5% BG showed that the amplitude force reduction was decreased from 11.1% and 12.9% at 2 cm to 7.1% and 6.5%, respectively. These values correlate very well with the 50% decrease in the BG thickness. Results for 1 cm thick 5.6% AMC are shown in Figs. 10a and b.

The results shown in Figs. 10 were surprising and rather counter-intuitive. The average amplitude force reduction of 1 cm 5.6% AMC was 33.5% which is the approximately the same value as measured for the 2 cm samples by reducing the difference of the change in the distance. ( $\sim 2\%$  like shown for water). Moreover the average impulse reduction is 24%, which again is within the range of values measured for the 2 cm specimens. Intriguingly, the power spectrum analysis shows that the attenuation coefficient at 1 cm is almost twice than the attenuation coefficient calculated according the 2 cm thickness. This finding shows that the main attenuation mechanism of AMC under impact is not based on the decay of waves while traveling through a viscous medium. The similar force mitigation shown for 1 and 2 cm demonstrates that for AMC, the attenuation is not a function of the thickness. For this situation, the common presentation of attenuation coefficient ( $\text{Np/cm}$ ) is not suitable for AMC solutions under impact, hence the attenuation cannot be divided by the AMC thickness. According to these findings, one should relate the attenuation coefficient presented at Fig. 8 as suitable only to a thickness of 2 cm. Experiments with 10% AMC at 1 cm have also shown similar behavior those presented at 2 cm thickness for the 10% AMC.

Additional work is currently performed to explore the existence of minimum thickness (if at all) for which the attenuation properties remain independent of the gel layer's thickness.

#### 4. Conclusions

This research was primarily motivated by the growing need to reduce the extent of damage to living tissues and vital organs, caused by blunt shock trauma. In the continued quest to find new methodologies to mitigate stress waves, the recent discovery that MC gelation can occur upon impact by fast impact energy uptake, has rendered AMC solutions the preferred candidates for the exploration reported herein.

Ultrasonic experiments show that the attenuation coefficients of AMC and BG at concentrations of 5.6% wt. are in the range of 0.1–0.2  $\text{Np/cm}$ , with a weak frequency dependence on the frequency. At higher concentrations, both materials exhibit higher attenuation, with stronger frequency dependence. As they cool down, AMC hydrogels show abnormal behavior of the attenuation coefficient in the frequencies at the range of 0.75–0.95 MHz. In this range, colder gels display higher attenuation of the ultrasound waves than hotter gels. It is currently assumed that this phenomenon is based on the ultrasound-induced network recruitment of solvated polymers, but further investigation into this proposed mechanism is required.

5.6% AMC shows very high efficiency in attenuating impacts and

shocks, which can be even further improved by increasing the polymer concentration to 10% wt. This improvement is quantified by amplitude force mitigation of 65.5% and decrease in the impulse ratio of 43.5%. These values are rather surprising since the 10% AMC consists of 90% water, which is a non-attenuating material. Moreover the calculated attenuation coefficient exhibits exponential increase with frequency upon impact, in contrast to the common linear correlation relation familiar from ultrasound experiments. Further examination of AMC at concentration of 10% wt. have shown an improved performance in comparison to the other tested materials,

Study of the AMC attenuation performance at 1 cm thickness yielded similar force and impulse mitigation as observed for 2 cm thickness. The fact which for AMC the energy mitigation is not a function of the thickness, emphasizes the unique ability of AMC to gel upon impact, through a reversible endothermic transition. This abnormality leads to a case where the common presentation of normalized attenuation coefficient with respect to the medium thickness is misleading and irrelevant.

The results of the study reported here are, in our view, novel when compared to the performance of other materials employed in applications of shock attenuation. Naturally, there are still more properties to explore and several abnormal findings which require further investigation. However, we hope that these findings will help pave the way to introducing these inverse-freezing materials to fields and applications into which they have not yet been combined.

#### Declaration of Competing Interest

The authors declare no conflict of interests. G. P., Y. R. and D. R. are the inventors of a PCT application by the Technion, number PCT/IL2018/050606, "Inverse-freezing compositions and use thereof".

#### Acknowledgment

This research was supported by the Technion Security Science and Technology Center, Grant 2024374, and by the Israel Innovation Authority, Nofar Program for R&D, case number 62155.

#### Supplementary materials

Supplementary material associated with this article can be found, in the online version, at doi:[10.1016/j.ijimpeng.2019.103392](https://doi.org/10.1016/j.ijimpeng.2019.103392).

#### References

- [1] Gondusky JS, Reiter MP. Protecting military convoys in Iraq: an examination of battle injuries sustained by a mechanized battalion during operation Iraqi freedom ii. *Mil Med* 2005;170(6):546–9.
- [2] Jones KD, Young T, Leppma M. Mild traumatic brain injury and posttraumatic stress disorder in returning iraq and afghanistan war veterans: implications for assessment and diagnosis. *J Couns Dev* 2010;88(3):372–6.

[3] Hayda R, Harris RM, Bass CD. Blast injury research: modeling injury effects of landmines, bullets, and bombs. *Clin Orthop Relat Res* 2004;422:97–108.

[4] Phillips YY. Primary blast injuries. *Ann Emerg Med* 1986;15(12):1446–50.

[5] Mac Donald CL, Johnson AM, Cooper D, Nelson EC, Werner NJ, Shimony JS, Snyder AZ, Raichle ME, Witherow JR, Fang R. Detection of blast-related traumatic brain injury in us military personnel. *New Engl J Med* 2011;364(22):2091–100.

[6] Roberts JC, O'connor JV, Ward EE. Modeling the effect of nonpenetrating ballistic impact as a means of detecting behind-armor blunt trauma. *J Trauma Acute Care Surgery* 2005;58(6):1241–51.

[7] DeKosky ST, Ikonomovic MD, Gandy S. Traumatic brain injury—football, warfare, and long-term effects. *New Engl J Med* 2010;363(14):1293–6.

[8] Amen DG, Wu JC, Taylor D, Willeumier K. Reversing brain damage in former nfl players: implications for traumatic brain injury and substance abuse rehabilitation. *J Psychoact Drugs* 2011;43(1):1–5.

[9] Verbitsky O, Mizrahi J, Voloshin A, Treiger J, Isakov E. Shock transmission and fatigue in human running. *J Appl Biomech* 1998;14(3):300–11.

[10] Alghamdi A. Collapsible impact energy absorbers: an overview. *Thin-walled Struct* 2001;39(2):189–213.

[11] Mukai T, Kanahashi H, Higashi K, Miyoshi T, Mabuchi M, Nieh T. Experimental study of energy absorption in a close-celled aluminum foam under dynamic loading. *Scr Mater* 1999;40(8).

[12] Levy D, Shirizly A, Rittel D. Static and dynamic comprehensive response of additively manufactured discrete patterns of Ti6Al4V. *Int J Impact Eng* 2018;122:182–96.

[13] Ozdemir Z, Hernandez-Nava E, Tyas A, Warren JA, Fay SD, Goodall R, Todd I, Askes H. Energy absorption in lattice structures in dynamics: experiments. *Int J Impact Eng* 2016;89:49–61.

[14] Santosa SP, Wierzbicki T, Hanssen AG, Langseth M. Experimental and numerical studies of foam-filled sections. *Int J Impact Eng* 2000;24(5):509–34.

[15] Rahimzadeh T, Arruda EM, Thouless M. Design of armor for protection against blast and impact. *J Mech Phys Solids* 2015;85:98–111.

[16] Hibbler R, Hibbeler RC, Hibbeler R. Engineering mechanics: statics and dynamics. MacMillan Publishing Company; 1992.

[17] Roland C, Fragiadakis D, Gamache R. Elastomer–steel laminate armor. *Compos Struct* 2010;92(5):1059–64.

[18] Tasdemirci A, Tunusoglu G, Güden M. The effect of the interlayer on the ballistic performance of ceramic/composite armors: experimental and numerical study. *Int J Impact Eng* 2012;44:1–9.

[19] Rijensky O, Rittel D. Polyurea coated aluminum plates under hydrodynamic loading: does side matter. *Int J Impact Eng* 2016;98:1–12.

[20] Ritter T, Geng X, Shung KK, Lopath PD, Park S-E, Shrout TR. Single crystal PZN/PT-polymer composites for ultrasound transducer applications. *IEEE Trans Ultrason Ferroelectr Freq Control* 2000;47(4):792–800.

[21] Cui L, Kiernan S, Gilchrist MD. Designing the energy absorption capacity of functionally graded foam materials. *Mater Sci Eng* 2009;507(1–2):215–25.

[22] Yu H, Guo Z, Li B, Yao G, Luo H, Liu Y. Research into the effect of cell diameter of aluminum foam on its compressive and energy absorption properties. *Mater Sci Eng* 2007;45:542–6.

[23] Enelund M, Mähler L, Runesson K, Josefson BL. Formulation and integration of the standard linear viscoelastic solid with fractional order rate laws. *Int J Solids Struct* 1999;36(16):2417–42.

[24] Hernández-Jiménez A, Hernández-Santiago J, Macias-Garcia A, Sánchez-González J. Relaxation modulus in pmma and ptfe fitting by fractional maxwell model. *Polym Test* 2002;21(3):325–31.

[25] Fancey KS. A mechanical model for creep, recovery and stress relaxation in polymeric materials. *J Mater Sci* 2005;40(18):4827–31.

[26] Guo A, Javni I, Petrovic Z. Rigid polyurethane foams based on soybean oil. *J Appl Polym Sci* 2000;77(2):467–73.

[27] Ahmed EM. Hydrogel: preparation, characterization, and applications: a review. *J Adv Res* 2015;6(2):105–21.

[28] Wackerling J, Schirhagl R. Applications of molecularly imprinted polymer nanoparticles and their advances toward industrial use: a review. *Anal Chem* 2015;88(1):250–61.

[29] Snyder WE, Clair JS. Conductive elastomers as sensor for industrial parts handling equipment. *IEEE Trans Instrum Meas* 1978;27(1):94–9.

[30] Parkinson W, Sisman O. The use of plastics and elastomers in nuclear radiation. *Nucl Eng Des* 1971;17(2):247–80.

[31] Brown E, Forman NA, Orellana CS, Zhang H, Maynor BW, Betts DE, DeSimone JM, Jaeger HM. Generality of shear thickening in dense suspensions. *Nat Mater* 2010;9(3):220.

[32] Lee YS, Wetzel ED, Wagner NJ. The ballistic impact characteristics of Kevlar® woven fabrics impregnated with a colloidal shear thickening fluid. *J Mater Sci* 2003;38(13):2825–33.

[33] Wagner N, Wetzel E. Advanced body armor utilizing shear thickening fluids. *United States Patent US72268782007*, 5.

[34] Parvari G, Rotbaum Y, Eichen Y, Rittel D. Impact-induced gelation in aqueous methylcellulose solutions. *Chem Commun* 2018;54(89):12578–81.

[35] Schupper N, Shnerb NM. Inverse melting and inverse freezing: a spin model. *Phys Rev E* 2005;72(4):046107.

[36] Rotbaum Y, Parvari G, Eichen Y, Rittel D. Static and dynamic large strain properties of methyl cellulose hydrogels. *Macromolecules* 2017;50(12):4817–26.

[37] Shepherd C, Appleby-Thomas G, Hazell P, Allsop D. In The dynamic behavior of ballistic gelatin, AIP conference proceedings. AIP; 2009. p. 1399–402. 2009.

[38] Swain M, Kieser D, Shah S, Kieser J. Projectile penetration into ballistic gelatin. *J Mech Behav Biomed Mater* 2014;29:385–92.

[39] Farrer AI, Odéen H, de Bever J, Coats B, Parker DL, Payne A, Christensen DA. Characterization and evaluation of tissue-mimicking gelatin phantoms for use with mrgus. *J Ther Ultrasound* 2015;3(1):9.

[40] Salisbury C, Cronin D. Mechanical properties of ballistic gelatin at high deformation rates. *Exp Mech* 2009;49(6):829–40.

[41] Kwon J, Subhash G. Compressive strain rate sensitivity of ballistic gelatin. *J Biomech* 2010;43(3):420–5.

[42] Rose JL. Ultrasonic waves in solid media. Cambridge: University Press; 2004.

[43] Chen C-h. Ultrasonic and advanced methods for nondestructive testing and material characterization. World Scientific; 2007.

[44] Blitz J. Ultrasonics: methods and applications. 1971.

[45] Hahn SL. Hilbert transforms in signal processing. Artech House; 1996.

[46] He P. Measurement of acoustic dispersion using both transmitted and reflected pulses. *J Acoust Soc Am* 2000;107(2):801–7.

[47] Kolsky H. An investigation of the mechanical properties of materials at very high rates of loading 62. IOP Publishing; 1949. p. 676.

[48] Rotbaum Y, Puici C, Rittel D, Domingos M. Quasi-static and dynamic in vitro mechanical response of 3D printed scaffolds with tailored pore size and architectures. *Mater Sci Eng* 2019;96:176–82.

[49] Richler D, Rittel D. On the testing of the dynamic mechanical properties of soft gelatins. *Exp Mech* 2014;54(5):805–15.

[50] Kuc R, Schwartz M. Estimating the acoustic attenuation coefficient slope for liver from reflected ultrasound signals. *IEEE Trans Sonics Ultrasonics* 1979;26(5):353–61.

[51] Dunn F. Attenuation and speed of ultrasound in lung: dependence upon frequency and inflation. *J Acoust Soc Am* 1986;80(4):1248–50.

[52] Kak AC, Dines KA. Signal processing of broadband pulsed ultrasound: measurement of attenuation of soft biological tissues. *IEEE Trans Biomed Eng* 1978(4):321–44.

[53] Verhoef WA, Cloostermans MJ, Thijssen JM. Diffraction and dispersion effects on the estimation of ultrasound attenuation and velocity in biological tissues. *IEEE Trans Biomed Eng* 1985;7(5):521–9.

[54] Kuc R, Taylor KJ. Variation of acoustic attenuation coefficient slope estimates for in vivo liver. *Ultrasound Med Biol* 1982;8(4):403–12.

[55] Marsden JE, Hughes TJ. Mathematical foundations of elasticity. Courier Corporation; 1994.

[56] Gould PL, Feng Y. Introduction to linear elasticity. Springer; 1994.

[57] Sanborn B, Song B, Nishida E, Knight M. Experimental evaluation of low-pass shock isolation performance of elastomers using frequency-based kolsky bar analyses. *Latin Am J Solids Struct* 2017;14(3):560–74.

[58] Chen W, Song B. Split hopkinson (Kolsky) bar: design, testing and applications. Springer; 2011.

[59] McAllister JW, Lott JR, Schmidt PW, Sammler RL, Bates FS, Lodge TP. Linear and nonlinear rheological behavior of fibrillar methylcellulose hydrogels. *ACS Macro Lett* 2015;4(5):538–42.

[60] Bodvik R, Dedenite A, Karlson L, Bergström M, Bäverbäck P, Pedersen JS, Edwards K, Karlsson G, Varga I, Claesson PM. Aggregation and network formation of aqueous methylcellulose and hydroxypropylmethylcellulose solutions. *Colloids Surfaces A* 2010;354(1):162–71.

[61] Patel TR, Morris GA, de la Torre JG, Ortega A, Mischnick P, Harding SE. Molecular flexibility of methylcelluloses of differing degree of substitution by combined sedimentation and viscosity analysis. *Macromol Biosci* 2008;8(12):1108–15.

[62] Lott JR, McAllister JW, Arvidson SA, Bates FS, Lodge TP. Fibrillar structure of methylcellulose hydrogels. *Biomacromolecules* 2013;14(8):2484–8.

[63] Desbrieres J, Hirrien M, Rinaudo M. A calorimetric study of methylcellulose gelation. *Carbohydr Polym* 1998;37(2):145–52.

[64] Chatterjee T, Nakatani AI, Adden R, Brackhagen M, Redwine D, Shen H, Li Y, Wilson T, Sammler RL. Structure and properties of aqueous methylcellulose gels by small-angle neutron scattering. *Biomacromolecules* 2012;13(10):3355–69.

[65] Rotbaum Y, Parvari G, Eichen Y, Rittel D. Mechanical reinforcement of methylcellulose hydrogels by rigid particle additives. *Mech Mater* 2019;132:57–65.

[66] Ramirez B, Misra U, Gupta V. Viscoelastic foam-filled lattice for high energy absorption. *Mech Mater* 2018;127:39–47.

[67] Hoshizaki TB, Brien SE. The science and design of head protection in sport. *Neurosurgery* 2004;55(4):956–67.

[68] Doengi F, Burnage S, Cottard H, Roumeas R. Lander shock-alleviation techniques. *ESA Bulletin* 1998;93:2.

[69] Li L, Shan H, Yue C, Lam Y, Tam K, Hu X. Thermally induced association and dissociation of methylcellulose in aqueous solutions. *Langmuir* 2002;18(20):7291–8.

[70] Arvidson S, Lott J, McAllister J, Zhang J, Bates F, Lodge T, Sammler R, Li Y, Brackhagen M. Interplay of phase separation and thermoreversible gelation in aqueous methylcellulose solutions. *Macromolecules* 2012;46(1):300–9.

[71] Sarkar N. Thermal gelation properties of methyl and hydroxypropyl methylcellulose. *J Appl Polym Sci* 1979;24(4):1073–87.